AIAA JOURNAL
Vol. 31, No. 11, November 1993

Locally Implicit Total Variation Diminishing Schemes on Mixed Quadrilateral-Triangular Meshes

C. J. Hwang* and S. Y. Yang†
National Cheng Kung University, Tainan, Taiwan, Republic of China

Locally implicit total variation diminishing schemes on mixed quadrilateral-triangular static/dynamic meshes have been developed to study steady and unsteady flows, respectively. In a Cartesian coordinate system, the Euler equations are solved by using a cell-centered finite volume algorithm. For steady inviscid flows, the efficiency and accuracy of the present approach are confirmed by investigating the oblique shock reflection at a wall and transonic flow around an NACA 0012 airfoil. To treat unsteady flow problems with moving boundaries, a new dynamic mesh algorithm, which saves memory, is efficient, and maintains quality, is presented in this paper. For analyzing the unsteady transonic flow around an NACA 0012 airfoil that pitches harmonically about the quarter chord, a quadrilateral-triangular dynamic mesh system is used. The calculated instantaneous pressure distributions and lift and moment coefficients during a cycle of motion compare well with related numerical and experimental data.

Introduction

RECENTLY, there has been much attention given to the use and development of mixed quadrilateral-triangular meshes and related numerical approaches.[1-4] Thornton and Vemaganti[1] presented a finite element remeshing approach that uses quadrilateral elements where possible, and triangles are introduced as needed. For problems with highly localized solution variation, this approach gives smaller solution errors with fewer unknowns than refinement of uniform, structured meshes. Ramakrishnan et al.[2] developed a refinement procedure based on quadrilateral elements that uses triangles to make a transition from crude to fine elements. On these kinds of quadrilateral and triangular meshes, the four-step Galerkin-Runge-Kutta scheme was employed to study the hypersonic flow over a cowl leading edge. It was found that the shocks and discontinuities were modeled with good resolution. To use the advantages of structured and unstructured approaches, Weatherill[3] created cell-centered and cell-vertex schemes on mixed quadrilateral-triangular meshes, where second- and fourth-order dissipation terms were used. From numerical experiments, this hybrid approach was accurate and efficient. In addition to centered difference types of schemes, an implicit upwind relaxation Euler solver on the polygonal finite volumes was presented by Struijs et al.[4] For supersonic channel flow, the refinement algorithm divides a triangle into three quadrilaterals, and mixed quadrilateral-triangular meshes are created. As shown in Ref. 4, the shock structures are clearly predicted. Even though significant progress has been achieved, the previous works do not include moving boundary effects. In this paper, locally implicit total variation diminishing (TVD) schemes, which were originally formulated on unstructured triangular static meshes,[5] are modified and extended to the mixed quadrilateral-triangular static and dynamic meshes. With and without considering the moving boundary, unsteady and steady inviscid flow calculations are performed.

In the unsteady flow calculations, such as those of transonic flows around oscillating airfoils,[6-8] considerable efforts have been expended to use a dynamic grid. On structured quadrilateral meshes, Venkatakrishnan and Jameson[6] introduced the finite volume scheme to solve the Euler equations for a moving domain. In this approach, a rigid mesh moving with the airfoil was used. By implementing a dynamic mesh algorithm on unstructured triangular cells, Batina[7] presented two methods—a Runge-Kutta time-stepping scheme with a finite-volume spatial discretization and an Euler time-integration scheme with upwind-biased spatial discretization—to analyze unsteady inviscid aerodynamics of oscillating airfoils. Grid points on the outer boundary were held fixed, and the instantaneous locations of the points on the body were prescribed. Also, this moving mesh satisfied the geometric conservation law. Furthermore, Batina[8] used implicit flux-split Euler schemes for unsteady aerodynamic analysis involving unstructured dynamic triangular meshes. In the present work, a new dynamic quadrilateral-triangular mesh algorithm that permits grid deformation to fit both moving and fixed boundaries simultaneously is presented. This algorithm can move the mesh smoothly as the airfoil pitches, and it saves memory, is efficient, and maintains quality.

The purpose of this paper is to construct a numerical solution procedure for investigating steady and unsteady compressible inviscid flows. The procedure includes 1) cell-centered, finite volume, symmetric TVD formulation on a mixed quadrilateral-triangular mesh, 2) adaptive mesh generation,[9] 3) locally implicit time integration with and without a moving mesh effect, and 4) a dynamic mesh algorithm. The Euler equations are solved in a Cartesian coordinate system. The steady calculations are performed on static quadrilateral-triangular meshes. The efficiency and accuracy of the present method are confirmed by studying the oblique shock reflection at a wall and transonic flow around an NACA 0012 airfoil. Finally, the TVD scheme and dynamic mesh algorithm are successfully applied to the transonic flow around an NACA 0012 airfoil pitching harmonically about the quarter chord.

Governing Equations

The unsteady flow of an inviscid fluid in a moving domain Ω with boundary $\partial\Omega$ is described by the Euler equations in integral form,

$$\frac{\partial}{\partial t}\int\int_{\Omega} W\,dx\,dy + \int_{\partial\Omega} \boldsymbol{F}\cdot d\boldsymbol{\ell} = 0 \tag{1}$$

where $\boldsymbol{F} = E\boldsymbol{i} + G\boldsymbol{j}$, $d\boldsymbol{\ell} = \boldsymbol{n}\,d\ell$, and $\boldsymbol{n}$ is the unit normal vector in the outward direction. The vectors of conserved variables

Received July 6, 1992; revision received Oct. 28, 1992; accepted for publication Nov. 2, 1992.

*Professor, Institute of Aeronautics and Astronautics, 1 University Road. Member AIAA.
†Graduate Student, Institute of Aeronautics and Astronautics, 1 University Road.

W and the convective fluxes E and G are given by

$$W = \begin{bmatrix} \rho \\ \rho u \\ \rho v \\ e \end{bmatrix}, \qquad E = \begin{bmatrix} \rho U \\ \rho U u + P \\ \rho U v \\ (e + P)U + x_t P \end{bmatrix} \tag{2}$$

$$G = \begin{bmatrix} \rho V \\ \rho V u \\ \rho V v + P \\ (e + P)V + y_t P \end{bmatrix}$$

where p, u, v, and e are the density, velocity components in the x and y directions, and total energy per unit volume, respectively. The U and V are defined by

$$U = u - x_t, \qquad V = v - y_t \tag{3}$$

where x_t and y_t are the grid speeds in the x and y directions, respectively. In this paper, pressure P is given by the equation of state for perfect gas.

Numerical Algorithm

By implementing a two-parameter family of symmetric TVD schemes[5] on the unstructured mixed quadrilateral-triangular static or dynamic meshes (see Fig. 1), Eq. (1) can be written as

$$\left(\frac{A^{n+1}\Delta W^n}{\Delta t}\right)_i + \frac{\theta}{1+\beta} Q_i(W^{n+1}) = -\frac{1-\theta}{1+\beta} Q_i(W^n) + \frac{\beta}{1+\beta} + \left(\frac{A^n \Delta W^{n-1}}{\Delta t}\right)_i - \left(\frac{W^n \Delta A^n}{\Delta t}\right)_i + \frac{\beta}{1+\beta}\left(\frac{W^{n-1}\Delta A^{n-1}}{\Delta t}\right)_i \tag{4}$$

where

$$\Delta W^m = W^{m+1} - W^m$$

$$\Delta A^m = A^{m+1} - A^m, \qquad m = n \quad \text{or} \quad n-1$$

$$Q_i = \int_{\partial\Omega} \boldsymbol{F} \cdot \mathrm{d}\underline{\ell}$$

In this paper, we choose $\theta = 1$ and $\beta = 0$ for steady calculations that are first-order accurate in time. For unsteady computation, $\theta = 1$ and $\beta = \frac{1}{2}$ are used, and the scheme becomes second-order accurate in time. The third and fourth terms on the right-hand side of Eq. (4) account for the effects of area variation when meshes deform during time evolution. Under rigid-body motions or mesh-fixed situations, these two terms will vanish.

In the present formulation, the numerical flux function Q_i is expressed as

$$Q_i(W) = \frac{1}{2}\sum_{k=1}^{IN} [(\boldsymbol{F}_i + \boldsymbol{F}_k) \cdot \mathrm{d}\underline{\ell}_{ik} - R_{ik}\Psi(\Lambda_{ik})(\Delta\alpha_{ik} - \Delta\tilde{\alpha}_{ik})] \tag{5}$$

where $IN = 3$ for triangular cell i and 4 for quadrilateral cell i.

The mathematical definitions and treatments of R_{ik}, Λ_{ik}, $\Delta\alpha_{ik}$, $\Delta\tilde{\alpha}_{ik}$, and $\Psi(\Lambda_{ik})$ are similar to those given in Ref. 5. In this paper, the interpolation for evaluating the "limiter" function $\Delta\tilde{\alpha}_{ik}$ is constructed by choosing the properties at cell edges and nodal points (see Fig. 1). At the cell edges, the properties are obtained by arithmetic average of the properties at adjacent cells. At the nodes, the properties are evaluated by the area-weighting rule.[5] The function Ψ has the following form:

$$\Psi(\Lambda_{ik}) = \begin{cases} |\Lambda_{ik}| & \text{if } |\Lambda_{ik}| \geq \epsilon_{ik} \\ \dfrac{(\Lambda_{ik}^2 + \epsilon_{ik}^2)}{2\epsilon_{ik}} & \text{otherwise} \end{cases} \tag{6}$$

where

$$\epsilon_{ik} = \xi[|(\boldsymbol{V} - \boldsymbol{V}_g) \cdot \mathrm{d}\underline{\ell}| + a\,|\mathrm{d}\underline{\ell}|]_{ik} I$$

$$\boldsymbol{V} = u\boldsymbol{i} + v\boldsymbol{j}$$

$$\boldsymbol{V}_g = x_t\boldsymbol{i} + y_t\boldsymbol{j}$$

$$I = \mathrm{diag}[1, 1, 1, 1]$$

In the previous equation, the variable a represents the sound speed, and ξ is a small positive coefficient taken as 0.1.

By using the Taylor series expansion, Eq. (4) is linearized and constructed in the delta form as follows:

$$L_i(\Delta W^n) = Res_i^n = -\frac{1}{1+\beta} Q_i(W^n) + \frac{\beta}{1+\beta}\left(\frac{A^n \Delta W^{n-1}}{\Delta t}\right)_i - \left(\frac{W^n \Delta A^n}{\Delta t}\right)_i + \frac{\beta}{1+\beta}\left(\frac{W^{n-1}\Delta A^{n-1}}{\Delta t}\right)_i - \frac{\theta}{2(1+\beta)}\sum_{k=1}^{IN} [(\boldsymbol{F}_i + \boldsymbol{F}_k)^n \cdot (\mathrm{d}\underline{\ell}^{n+1} - \mathrm{d}\underline{\ell}^n)] \tag{7}$$

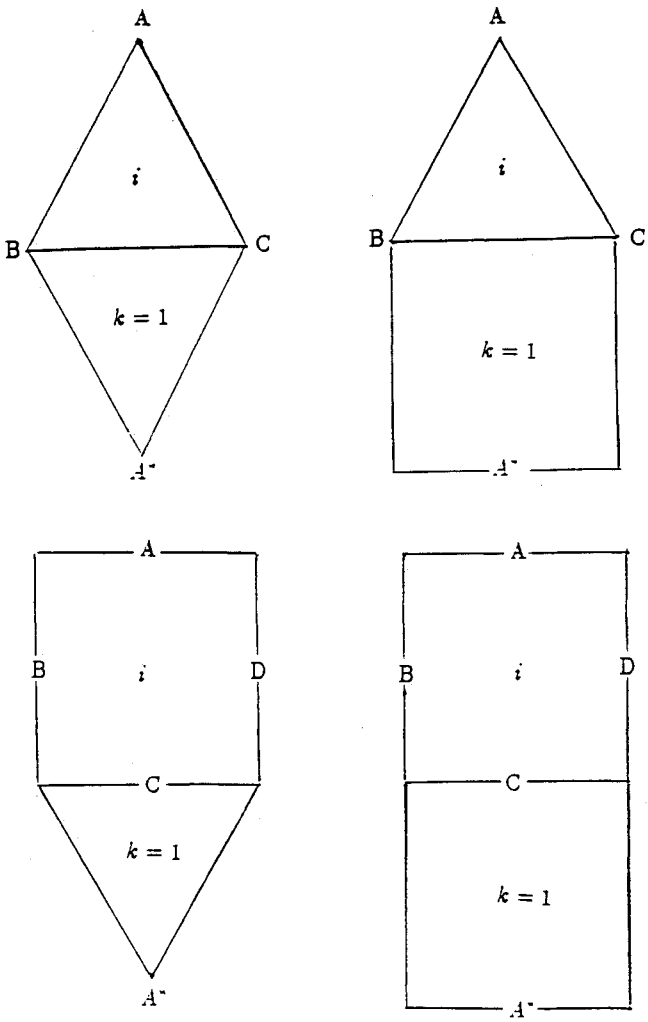

Fig. 1 Definition of unstructured mixed quadrilateral-triangular meshes for the cell-centered TVD schemes.

where

$$L_i(\Delta W^n) = CI\Delta W_i^n + \sum_{k=1}^{IN} CK_k \Delta W_k^n$$

and

$$CI = \left(\frac{A^{n+1}}{\Delta t}\right)_i I + \frac{\theta}{2(1+\beta)} \sum_{k=1}^{IN} \times \left[M_{ik} - R_{ik}\Psi(\Lambda_{ik})R_{ik}^{-1}\left(1 - \frac{\Delta\bar{\alpha}_{ik}}{\Delta\alpha_{ik}}\right)\right]^n$$

$$CK_k = \frac{\theta}{2(1+\beta)}\left[M_{ik} - R_{ik}\Psi(\Lambda_{ik})R_{ik}^{-1}\left(1 - \frac{\Delta\bar{\alpha}_{ik}}{\Delta\alpha_{ik}}\right)\right]^n$$

$$M_{ik}^n = \left(\frac{\partial \boldsymbol{F}^n}{\partial W} \cdot \mathrm{d}\underline{t}^{n+1}\right)_{ik}$$

The last term on the right-hand side of Eq. (7) arises from the dynamic mesh effects during linearization. To solve Eq. (7), a modified Gauss-Seidel scheme[5] is employed. In steady-state calculations, an implicit smoothing process, which was presented in Ref. 5, is applied and extended to mixed quadrilateral-triangular meshes. By using this process, the present schemes become more robust.

Boundary Conditions

For the steady flow calculations, no-penetration and adiabatic wall conditions are imposed at the body or wall surface. Pressure is estimated by using x- and y-momentum equations. For the oscillating airfoil flow calculation, velocity components perpendicular and parallel to the moving airfoil surface are expressed as

$$\tilde{V}_n = (u - x_t)\frac{\Delta y}{\Delta s} - (v - y_t)\frac{\Delta x}{\Delta s} \tag{8a}$$

$$\tilde{V}_t = (u - x_t)\frac{\Delta x}{\Delta s} + (v - y_t)\frac{\Delta y}{\Delta s} \tag{8b}$$

where $\Delta s^2 = \Delta x^2 + \Delta y^2$, and Δx and Δy are the directed length of edges for a boundary cell in the x and y coordinate directions, respectively. The $\tilde{V}_t$ is obtained from extrapolation, and $\tilde{V}_n = 0$ is imposed as the flow tangency boundary condition. After finishing the computations of $\tilde{V}_n$ and $\tilde{V}_t$, the Cartesian fluid velocity components u and v on the oscillating airfoil surface are obtained from

$$u = \tilde{V}_t\frac{\Delta x}{\Delta s} + \tilde{V}_n\frac{\Delta y}{\Delta s} + x_t \tag{9a}$$

$$v = \tilde{V}_t\frac{\Delta y}{\Delta s} - \tilde{V}_n\frac{\Delta x}{\Delta s} + y_t \tag{9b}$$

Pressure and density are obtained by extrapolation from the values at the interior cells. In the far field, one-dimensional characteristic analysis based on Riemann invariants is used to determine the values of the flow variables on the outer boundary of the computational domain.

Dynamic Mesh Algorithm and Geometric Conservation Law

A significant work of the present study is the creation of a new dynamic mesh algorithm, which saves memory, is efficient, and maintains quality. The concept of this dynamic mesh algorithm is similar to that of Batina.[7] To obtain displacements Δx_j and Δy_j at each interior node j of the grid, Batina[7] solved the static equilibrium equations in the x and y directions iteratively by using the predictor-corrector method. This method first predicts the displacements according to a linear extrapolation and then corrects these displacements by using several Jacobi iterations. The static equilibrium equations are given as

$$\Delta x_j = \frac{\sum K_l \Delta x_l}{\sum K_l} \tag{10a}$$

$$\Delta y_j = \frac{\sum K_l \Delta y_l}{\sum K_l} \tag{10b}$$

where K_l is the spring stiffness, and the summations in Eqs. (10) are performed over all edges of the mesh that have node j as an endpoint. In a Jacobi iteration, the values of displacements at the nodes that surround node j are at the previous level, whereas some of them are replaced by the values at the latest level if a Gauss-Seidel iteration is used. To reduce the number of iterations and accelerate convergence, a new approach, which is based on the modified Gauss-Seidel method,[5,10] is created to solve Eqs. (10) in the present work. The calculation for a symmetric cycle of iterative corrections is performed by starting at the first interior node and sweeping to the latest interior node followed by an opposite sweep. Thus, for each interior node j, Eqs. (10) is rewritten as

$$^3/_2\, C\, \mathrm{d}x_j = L_x(\Delta x^*) \tag{11a}$$

$$^3/_2\, C\, \mathrm{d}y_j = L_y(\Delta y^*) \tag{11b}$$

and

$$\Delta x_j^{m+1} = \Delta x_j^m + G_{in}\, \mathrm{d}x_j \tag{12a}$$

$$\Delta y_j^{m+1} = \Delta y_j^m + G_{in}\, \mathrm{d}y_j, \qquad m = 1, 2 \tag{12b}$$

where

$$C = \left(\sum K_l\right)$$

$$L_x(\Delta x^*) = \sum K_l \Delta x_l^* - C\Delta x_j^*$$

$$L_y(\Delta y^*) = \sum K_l \Delta y_l^* - C\Delta y_j^*$$

The coefficient G_{in} is the relaxation parameter. The variables Δx^* and Δy^* shown on the right-hand sides of Eqs. (11) take the latest available values from Eqs. (12). That is, the values of Δx_l^*, Δx_j^*, Δy_l^*, or Δy_j^* are at m or $m+1$ depending on the sweeping pattern. Whenever the corrections $\mathrm{d}x_j$ and $\mathrm{d}y_j$ are evaluated from Eq. (11), the displacements Δx_j and Δy_j in Eqs. (12) are updated simultaneously for each interior node j. Except for the memory to store Δx_j and Δy_j, it is not necessary to use extra memory, such as the storage required for the predictor step in the predictor-corrector procedure.[7] Therefore, the present dynamic mesh algorithm saves memory.

To maintain the quality (smoothness) of the moving mesh, several symmetric cycles are performed until a convergence state is obtained. In the present calculation, convergence is assumed to be achieved when absolute values of $\mathrm{d}x_j$ and $\mathrm{d}y_j$ are both less than a selected small value δ for all interior nodes. Because of the characteristics of the modified Gauss-Seidel method,[5,10] the number of iterations to achieve a mesh convergence criterion will be less than that for the conventional Gauss-Seidel method. In the present calculation, the average values of the cycle of iterations to achieve the mesh convergence criterion ($\delta = 10^{-7}$, $G_{in} = 1.0$) for modified and conventional Gauss-Seidel methods are equal to 4.65 and 8.24, respectively. Therefore, the efficiency of the present method is

confirmed. At the end of a time step, the new locations of the interior nodes are determined by

$$x_j^{n+1} = x_j^n + \Delta x_j \tag{13a}$$

$$y_j^{n+1} = y_j^n + \Delta y_j \tag{13b}$$

To further investigate the characteristics of the present dynamic mesh algorithm, different values of δ and G_{in} are selected. When the values of δ and G_{in} are equal to 10^{-6} and 1.0, respectively, it takes 1.11 average cycles of iterations to achieve the convergence state. If δ is equal to 10^{-7} and two different values of G_{in}—1.2 and 1.4—are used, 4.35 and 4.21 average cycles of iterations are required to achieve the convergence state, respectively. From the previous discussion, the present dynamic mesh algorithm saves memory and is efficient in maintaining the mesh quality. Also, it is completely general to treat realistic aerodynamic motions.

In addition to the mass, momentum, and energy conservation laws that govern the physics of the flow, a geometric conservation law needs to be satisfied numerically. As discussed in Ref. 11, the geometric conservation law is defined by

$$\frac{\partial}{\partial t}\int\int_{\Omega} dA = \frac{\Delta A}{\Delta t} = \int_{\partial\Omega} \underline{V}_g \cdot d\underline{\ell} \tag{14}$$

where ΔA is determined from the new and old mesh positions. The flux due to grid speed $\underline{V}_g \cdot d\underline{\ell}$, which has appeared in some of the aforementioned equations, is then determined from Eq. (14).

Mesh Generation Techniques

For the steady flow calculations in this paper, the adaptive mixed quadrilateral-triangular static meshes are generated by the global remeshing algorithm.[9] When the flow around an oscillating airfoil is studied, the dynamic quadrilateral-triangular mesh is used. The quadrilaterals are created first by stretching a proper distance from the airfoil surface in the outward normal direction, and unstructured triangles are distributed elsewhere according to the remeshing algorithm.[9] The mixed mesh with a layer of structured quadrilaterals on the airfoil surface is appropriate to simulate the boundary-layer effects when the viscous flows are studied in the future work.

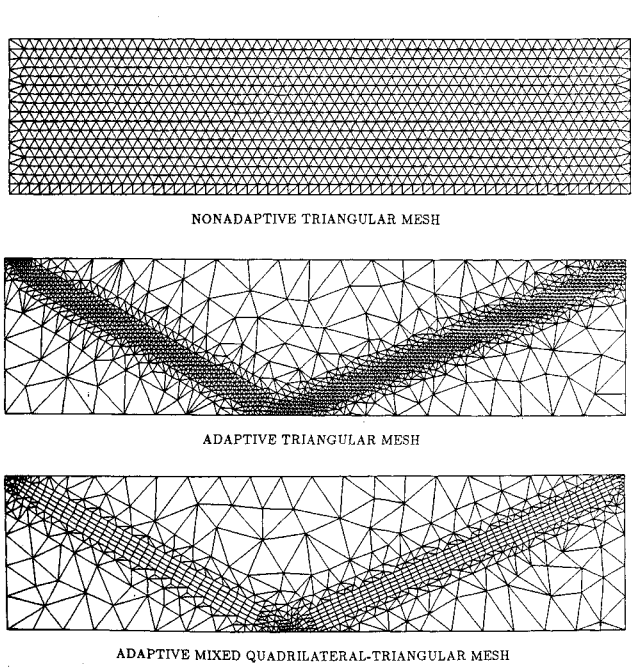

Fig. 2 Meshes for the oblique shock reflection at a wall: nonadaptive triangles (2020 elements), adaptive triangles (2803 elements), and adaptive mixed quadrilateral-triangular mesh (1129 elements).

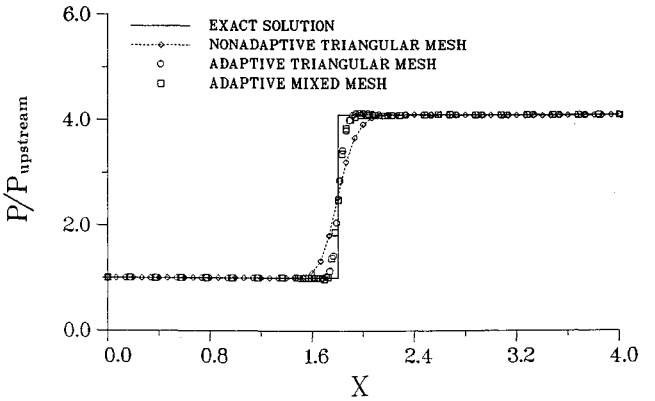

Fig. 3 Pressure distributions along the wall for oblique shock reflection.

Results and Discussion

On unstructured static meshes, the present symmetric TVD algorithm is evaluated by performing two steady flow calculations, which include the oblique shock reflection at a wall and transonic flow around an NACA 0012 airfoil. To further understand the characteristics of the current schemes, the unsteady flow calculation for the NACA 0012 airfoil pitching harmonically about the quarter chord is conducted on the dynamic quadrilateral-triangular mesh.

Oblique Shock Reflection at a Wall

In this flow problem, the freestream Mach number and incident shock angle are equal to 2.9 and 29 deg, respectively. To confirm the accuracy and reliability of the present scheme, three kinds of grid systems are employed. The meshes and corresponding pressure distributions are shown in Figs. 2 and 3, respectively. On the adaptive regular triangular and stretched mixed quadrilateral-triangular meshes, the incident and reflective shocks are clearly resolved. On the mixed mesh, the grid lines are almost aligned with the shock. As shown in Fig. 3, high-resolutional results that are obtained on the adaptive meshes compare well with exact solutions. In this work, steady-state solutions are assumed to be achieved when the L_2-norm of density is less than or equal to 10^{-6}. Also, density is selected as the key variable to decide the remeshing parameters.[9]

Transonic Flow Around an NACA 0012 Airfoil

To evaluate the present solution algorithm, transonic flow ($M_\infty = 0.8$) around an NACA 0012 airfoil with angle of attack ($\alpha = 1.25$ deg) is investigated. The outer boundary of the computational domain is located at 20 chord lengths away from the airfoil. Three different grid systems and corresponding pressure coefficient distributions are presented in Figs. 4 and 5, respectively. As shown in Fig. 5, the calculated pressure coefficient distributions compare well with the upwind TVD results of Yee and Harten[12] in which a structured C-grid with 249×41 quadrilateral points was used. It is apparent that accurate and high-resolutional results are obtained on the adaptive meshes.

To further understand the characteristics of the present solution-adapted procedure, the Courant-Friedrichs-Lewy (CFL), element number, iteration number, and CPU time in the previous steady flow calculations are given in Table 1. The generation of an adaptive mixed quadrilateral-triangular mesh takes a little more CPU time than that of an adaptive triangular mesh. However, the CPU time required to achieve steady-state flow solutions on the adaptive mixed mesh is less than that on the adaptive triangular mesh. According to the previous discussion and the data given in Table 1, the present TVD scheme, which is formulated on the mixed quadrilateral-triangular meshes, is accurate and efficient to treat steady flow

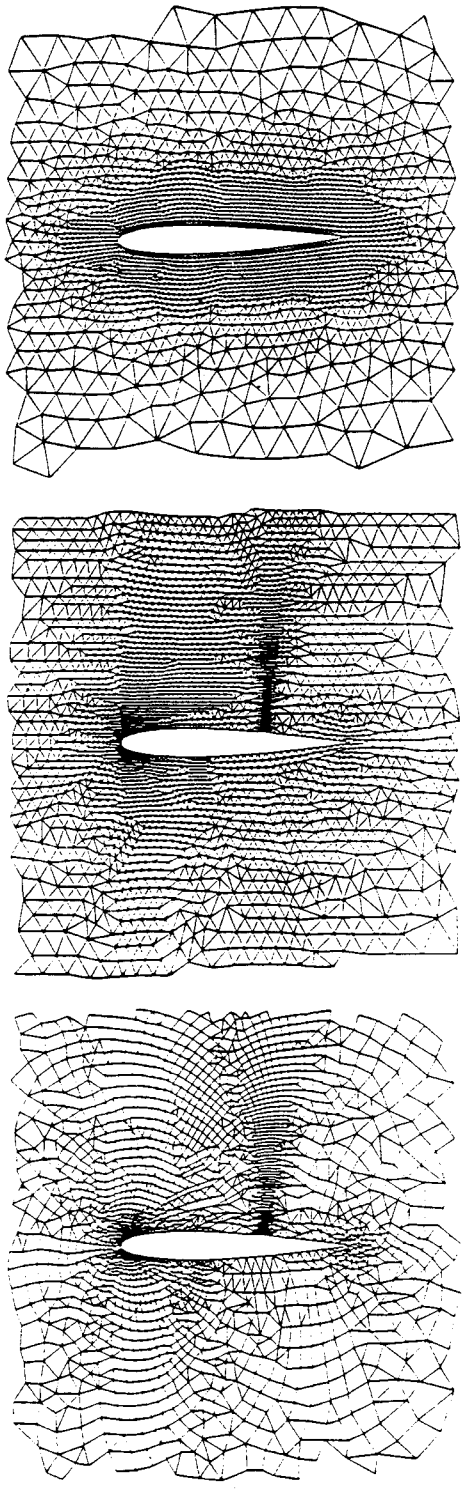

Fig. 4 Partial view of meshes for the NACA 0012 airfoil: a) nonadaptive triangular mesh (6154 elements), b) adaptive triangular mesh (10,772 elements), and c) adaptive mixed quadrilateral-triangular mesh (5386 elements).

problems. Fewer elements and iterations as well as reduced CPU time are evident.

Transonic Flow Around an Oscillating Airfoil

Unsteady results are obtained for the NACA 0012 airfoil pitching harmonically about the quarter chord with an amplitude of $\alpha_I = 2.51$ deg and a reduced frequency of $k = 0.0814$ based on semichord. The motion of the oscillating airfoil is governed by the relation

$$\alpha = \alpha_0 + \alpha_I \sin(\omega t) \tag{15}$$

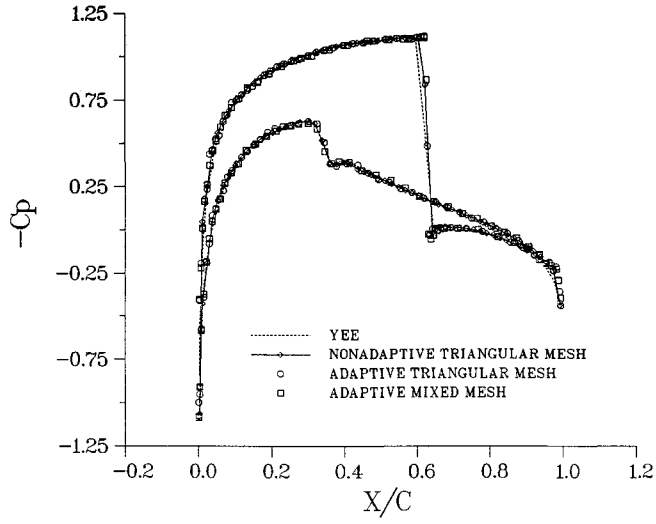

Fig. 5 Pressure coefficient distributions for transonic flow over the NACA 0012 airfoil ($M_\infty = 0.8$, $\alpha = 1.25$ deg).

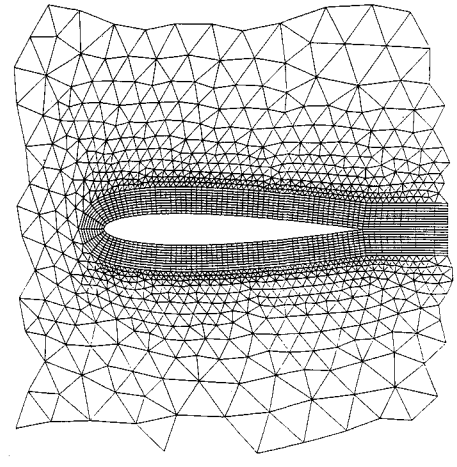

Fig. 6 Partial view of the mesh for the NACA 0012 airfoil pitching at $M_\infty = 0.755$, $\alpha_0 = 0.016$ deg, $\alpha_I = 2.51$ deg, and $k = 0.0814$.

where α is the instantaneous angle of attack. The frequency ω is related to the reduced frequency by the relation $k = \omega c/2V_\infty$, where c is the airfoil chord length. The solution for the airfoil at a freestream Mach number of $M_\infty = 0.755$ and an angle of attack of $\alpha_0 = 0.016$ deg is taken as the initial condition. In this case, the computational domain is taken to be $21c \times 20c$. The quadrilateral-triangular mesh system (see Fig. 6) contains 4688 elements and 3285 nodes, and there are 110 points that lie on the airfoil surface. For $\delta = 10^{-6}$ and $G_{in} = 1.0$, the present dynamic mesh algorithm is applied to deform the mesh smoothly during pitching motions.

By choosing a spatially constant marching time step in which the maximum value of CFL is equal to 30, three cycles of airfoil motion are processed to obtain a periodic solution, and each cycle contains about 1132 iterations. Compared with the related numerical results[8,13] and experimental data,[14] the calculated instantaneous surface pressure distributions at eight points in time during the third cycle of motion are shown in Figs. 7a–7h. Except for the pressure distributions given in Fig. 7a, the results during the first part (see Figs. 7a–7d) of the cycle demonstrate a shock wave on the upper surface of the airfoil, and the flow over the lower surface is predominantly subcritical. During the latter part (see Figs. 7e–7h) of the cycle (except Fig. 7e), the flow about the upper surface is subcritical, and a shock forms along the lower surface. The flow phenomena, which are shown in Figs. 7a and 7e, are due to the fact that the shock cannot move with the airfoil motion in the

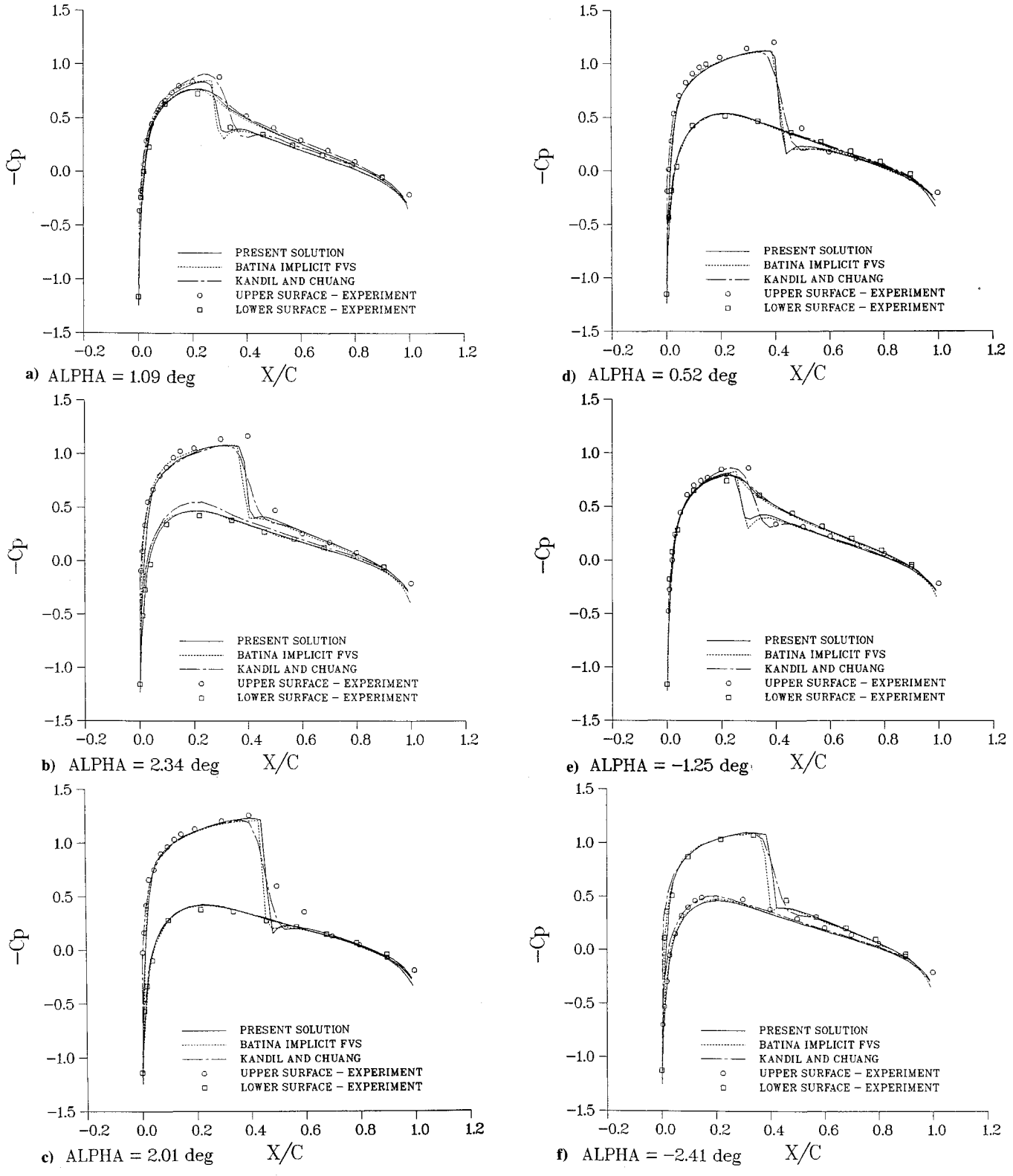

Fig. 7 Instantaneous pressure distributions for NACA 0012 airfoil pitching at $M_\infty = 0.755$, $\alpha_0 = 0.016$ deg, $\alpha_I = 2.51$ deg, and $k = 0.0814$.

same speed. In general, the present results compare well with experimental data,[14] and the profiles of pressure distribution are closer to the solutions of Batina[8] than those of Ref. 13. Also, the currently predicted shock position (see Fig. 7g) compares better with the adaptive solution[15] than the nonadaptive solution given in Ref. 8. Similar to the results presented in Refs. 8, 13, and 15, the present solutions indicate the expected symmetry in the flow. The upper surface pressure distribution during the first half of the cycle is very similar to the lower surface pressure distribution during the second half of the cycle, except for the reversal of the shock wave on the upper and lower surfaces. To further evaluate the present numerical approach, the lift and moment coefficients vs the instantaneous angle of attack are plotted in Fig. 8. The present lift coefficient distributions agree well with Batina's results,[8] but both of them differ from experimental data[14] equally. As mentioned by Batina,[8] the comparisons of lift coefficient indicate that the data were probably obtained at a higher effective

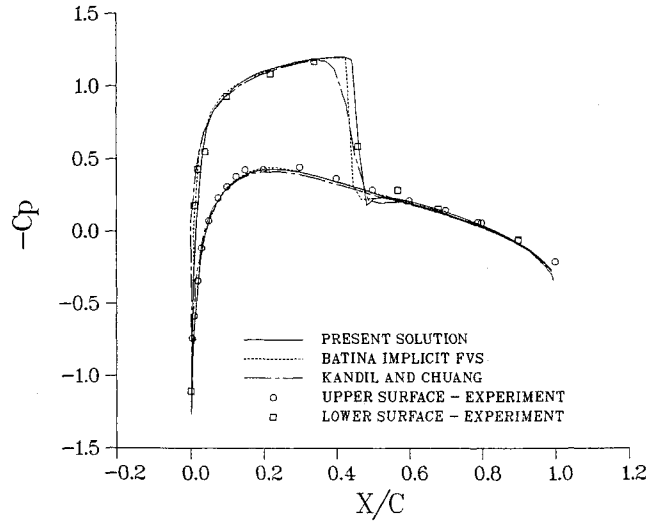

g) ALPHA = −2.0 deg

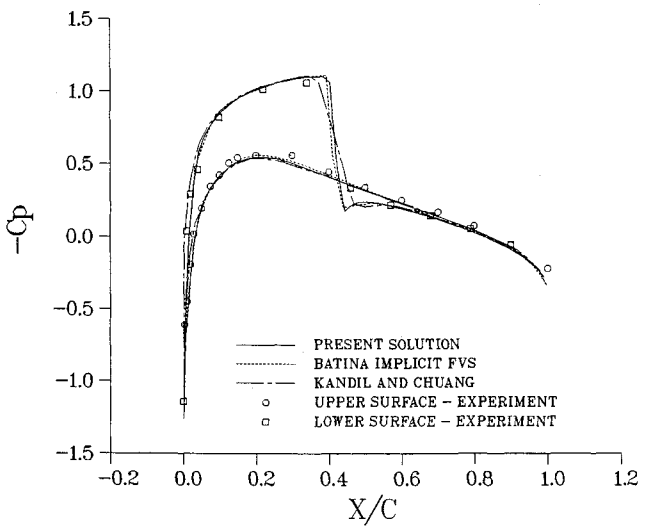

h) ALPHA = −0.54 deg

Fig. 7 (Continued) Instantaneous pressure distributions for NACA 0012 airfoil pitching at $M_\infty = 0.755$, $\alpha_0 = 0.016$ deg, $\alpha_I = 2.51$ deg, and $k = 0.0814$.

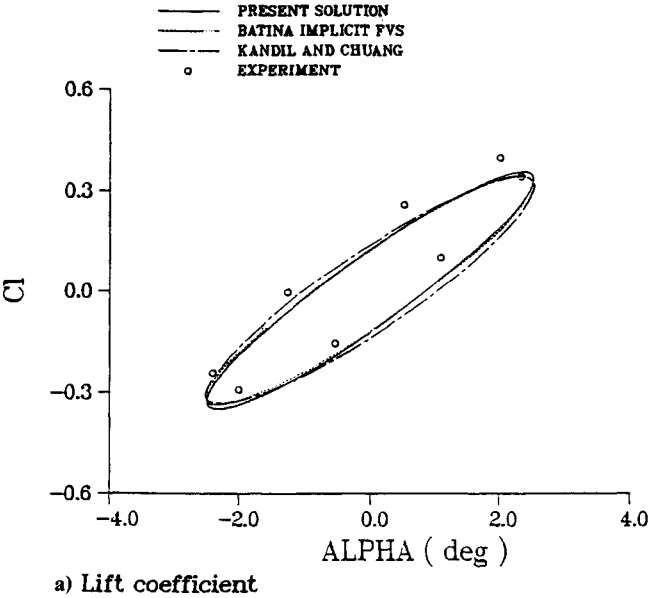

a) Lift coefficient

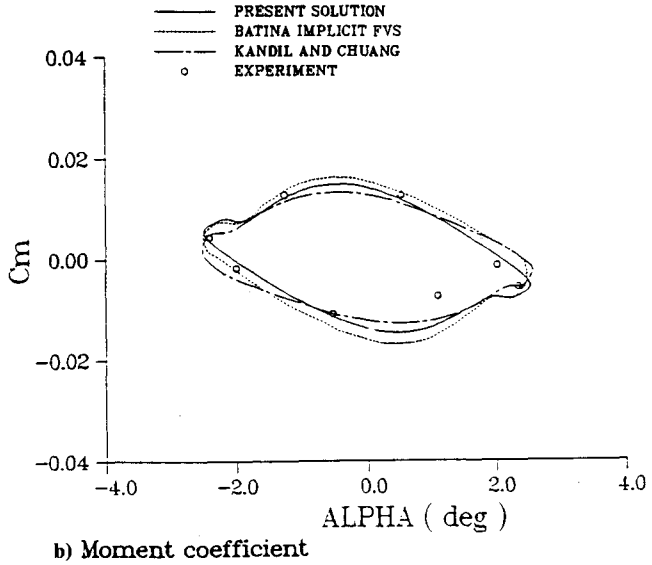

b) Moment coefficient

Fig. 8 a) Lift coefficient and b) moment coefficient vs instantaneous angle of attack for the NACA 0012 airfoil pitching at $M_\infty = 0.755$, $\alpha_0 = 0.016$ deg, $\alpha_I = 2.51$ deg, and $k = 0.0814$.

Table 1 CFL, element number, iteration number, and CPU time in steady flow calculations[a]

Case[b]	Mesh[c]	CFL	Element no.	Iteration no.	CPU[d], s	CPU[e], s
1	1	5	2,020	346	565	8
1	2	5	2,803	377	860	17
1	3	5	1,129	226	228	21
2	1	5	6,154	2526	12,149	33
2	2	5	10,772	3017	25,127	77
2	3	5	5,386	2640	12,661	89

[a]Calculations were done on a DEC 5000/200 workstation.
[b]The following two test cases are studied: 1) oblique shock reflection at a wall and 2) transonic flow around an NACA 0012 airfoil.
[c]The following three mesh systems are used: 1) nonadaptive triangular mesh, 2) adaptive triangular mesh, and 3) adaptive mixed quadrilateral-triangular mesh.
[d]Computational time required to obtain the steady solution.
[e]Computational time required to generate the mesh.

steady-state angle of attack since the experimental values are higher than the calculated values. From the previous discussion, the present dynamic mesh algorithm and locally implicit symmetric TVD scheme are reliable and suitable for studying unsteady flow problems with moving boundaries.

Conclusions

In this paper, locally implicit cell-centered finite volume TVD schemes have been developed to solve the unsteady Euler equations on mixed quadrilateral-triangular static/dynamic meshes. To simulate flow behavior with moving boundaries in the Cartesian coordinate system, a new dynamic mesh algorithm is presented. Based on numerical experiments, this algorithm saves memory, is efficient, and maintains quality. In steady flow calculations, the oblique shock reflection at a wall and the transonic flow around an NACA 0012 airfoil are studied. Nonadaptive and adaptive regular triangles and an adaptive mixed quadrilateral-triangular mesh are used. From the pressure distributions obtained, the number of elements used, number of iterations taken, and CPU time required for analysis, the present method that is formulated on the static mixed mesh is accurate and efficient. For the transonic flow around an NACA 0012 airfoil pitching harmonically about the quarter chord, the predicted pressure distributions and lift and moment coefficients during a cycle of motion give satisfactory comparison with related numerical and experimental data. The present solution algorithm is accurate and suitable for investigating steady and unsteady flows with complex geometries and/or moving boundaries.

References

[1]Thornton, E. A., and Vemaganti, G. R., "An Adaptive Remeshing Method for Finite Element Thermal Analysis," AIAA Paper 88-2662, June 1988.

[2]Ramakrishnan, R., Bey, K. S., and Thornton, E. A., "Adaptive Quadrilateral and Triangular Finite-Element Scheme for Compressible Flows," *AIAA Journal,* Vol. 28, No. 1, 1990, pp. 51–59.

[3]Weatherill, N. P., "Mixed Structured-Unstructured Meshes for Aerodynamic Flow Simulation," *The Aeronautical Journal,* Vol. 94, No. 934, 1990, pp. 111–123.

[4]Struijs, R., Vankeirsbilck, P., and Deconinck, H., "An Adaptive Grid Polygonal Finite Volume Method for the Compressible Flow Equations," AIAA Paper 89-1959, June 1989.

[5]Hwang, C. J., and Liu, J. L., "Locally Implicit Total-Variation-Diminishing Schemes on Unstructured Triangular Meshes," *AIAA Journal,* Vol. 29, No. 10, 1991, pp. 1619–1626.

[6]Venkatakrishnan, V., and Jameson, A., "Computation of Unsteady Transonic Flows by the Solution of Euler Equations," *AIAA Journal,* Vol. 26, No. 8, 1988, pp. 974–981.

[7]Batina, J. T., "Unsteady Euler Airfoil Solutions Using Unstructured Dynamic Meshes," *AIAA Journal,* Vol. 28, No. 8, 1990, pp. 1381–1388.

[8]Batina, J. T., "Implicit Flux-Split Euler Schemes for Unsteady Aerodynamic Analysis Involving Unstructured Dynamic Meshes," *AIAA Journal,* Vol. 29, No. 11, 1991, pp. 1836–1843.

[9]Hwang, C. J., and Wu, S. J., "Global and Local Remeshing Algorithms for Compressible Flows," *Journal of Computational Physics,* Vol. 102, No. 1, 1992, pp. 98–113.

[10]Reddy, K. C., and Jacocks, J. L., "A Locally Implicit Scheme for the Euler Equations," AIAA Paper 87-1144, June 1987.

[11]Vinokur, M., "An Analysis of Finite-Difference and Finite-Volume Formulations of Conservation Laws," *Journal of Computational Physics*, Vol. 81, No. 1, 1989, pp. 1–52.

[12]Yee, H. C., and Harten, A., "Implicit TVD Schemes for Hyperbolic Conservation Laws in Curvilinear Coordinates," *AIAA Journal,* Vol. 25, No. 2, 1987, pp. 266–274.

[13]Kandil, O. A., and Chuang, H. A., "Unsteady Transonic Airfoil Computation Using Implicit Euler Scheme on Body-Fixed Grid," *AIAA Journal,* Vol. 27, No. 8, 1989, pp. 1031–1037.

[14]Landon, R. H., "NACA 0012. Oscillatory and Transient Pitching," Compendium of Unsteady Aerodynamic Measurements, Data Set 3, AGARD-R-702, Aug. 1982.

[15]Rausch, R. D., Batina, J. T., and Yang, H. T. Y., "Spatial Adaptation of Unstructured Meshes for Unsteady Aerodynamic Flow Computations," *AIAA Journal,* Vol. 30, No. 5, 1992, pp. 1243–1251.